SCIENTIFIC REPORTS

OPEN

SUBJECT AREAS:
CHEMICAL PHYSICS
WETTING

Received
4 March 2014

Accepted
27 June 2014

Published
18 July 2014

Correspondence and requests for materials should be addressed to H.P.F. (fanghaiping@sinap.ac.cn)

Enhanced Permeation of a Hydrophobic Fluid through Particles with Hydrophobic and Hydrophilic Patterned Surfaces

Renliang Zhang[1], Yousheng Xu[2], Binghai Wen[3], Nan Sheng[1] & Haiping Fang[1]

[1]Division of Interfacial Water and Key Laboratory of Interfacial Physics and Technology, Shanghai Institute of Applied Physics, Chinese Academy of Sciences, Shanghai 201800, China, [2]School of Light Industry, Zhejiang University of Science and Technology, Hangzhou 310023, China, [3]College of Computer Science and Information Engineering, Guangxi Normal University, Guilin 541004, China.

The wetting properties of solid surfaces are significant in oil/gas and liquid displacement processes. It is difficult for hydrophobic fluids to permeate channels filled with hydrophilic particles and an aqueous phase, and this is thought to be the primary cause of low yields in low permeability reservoir operations. Using three-dimensional lattice Boltzmann simulations, we show that particles with hydrophobic and hydrophilic patterned surfaces can greatly improve hydrophobic fluid permeation. Specifically, a hydrophobic fluid can easily access micro-channels in the hydrophobic regions, which extend rapidly even to the hydrophilic regions and accelerate hydrophobic fluid escape. This work enriches understanding of multiphase flow in porous media at the pore scale and fracture conductivity and is expected to have great significance in the exploitation of low permeability reservoirs and shale gas.

Low permeability reservoirs are characterized by very low matrix permeability, minute pores and natural non-connected fractures, and thus have low natural industrial capacity. To improve the recovery efficiency of oil and gas, hydraulic fracturing is usually applied after wells are drilled[1]. Hydraulic fracturing is implemented by pumping large volumes of an aqueous phase containing suspended proppants into reservoirs under high pressure. The rocks around wells are split or fractured and the proppant particles infiltrate and support the fractures. Usually, the surfaces of proppant particles are hydrophilic so they can penetrate the fractures under the aqueous phase flow. Because of the strong attractive interactions between the aqueous phase and particles, the proppants will trap the injected aqueous phase and then form barriers preventing outflow (diffusion) of hydrophobic oil/gas. This phenomenon is called water blocking damage[2] and is the primary cause of low yields in low permeability reservoir developments during the middle-late stage[3–5]. It is clear that a key objective is to keep the proppant-water interaction strong enough, while allowing the hydrophobic fluid to flow (diffuse) rapidly near the proppant. Through the development of new synthesis techniques[6,7], it is becoming easier to decorate particle surfaces[8]. We propose that the presence of hydrophobic patterns on hydrophilic particle surfaces may greatly enhance permeation of the hydrophobic oil/gas in micro-channels. Because there would still be sufficient hydrophilic regions on the particles, interactions between the particles and aqueous phase would still be sufficient to enable its penetration into a fracture. On the other hand, there may be inhomogeneous wetting properties on the surfaces of natural rocks. Thus, it is also of great importance to study oil/gas permeation through fractures in such rocks.

In this paper, using a three-dimensional (3D) model, in which the channel is packed by particles with hydrophobic and hydrophilic patterned surfaces, we show that wettability-patterned particles can greatly enhance hydrophobic fluid permeation through a channel. We used a lattice Boltzmann method to perform numerical simulations and found that a hydrophobic fluid could easily displace an aqueous phase from the hydrophobic regions and opened micro-channels. In addition to hydrophobic fluid infiltration, these micro-channels extended rapidly even into the hydrophilic regions, resulting in elimination of blocking by the aqueous phase in the particle-packing region.

The geometry of the system is shown in Figure 1(a), together with a snapshot of some aqueous phase fluid. The length of the channel was 480 lattice units, while its cross-section was a 120×120 square array. Arrayed in two layers, 18 spherical particles were closely packed from $x = 130$ to 210 in the channel. The diameter of each spherical particle was 40 lattice units, and thus the volume of the packed porous medium was $80 \times 120 \times 120$. The non-slip bounce-back scheme was adopted for the particle boundary and channel wall, and a pressure boundary condition was employed at the inlet and outlet to drive fluid flow. Initially, the aqueous phase filled the space from

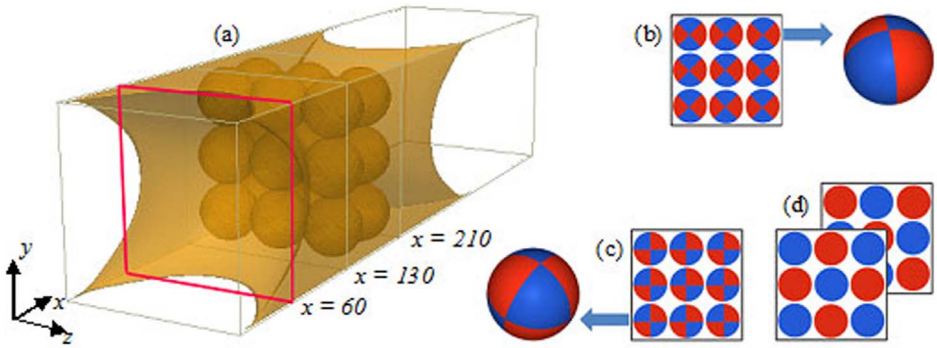

Figure 1 | (a) Schematic diagram illustrating water blocking, in which the light yellow denotes the aqueous phase in the initial equilibrium state. (b) Sketch of the wettability-patterned particles with two hydrophilic and two hydrophobic regions packed in a channel. (c) Sketch of wettability-patterned particles with four hydrophilic and four hydrophobic regions packed in a channel. (d) Sketch of the mixed hydrophobic and hydrophilic particles packed in the channel. The red parts indicate hydrophobic regions, with an intrinsic contact angle of 117.7 degrees, whereas the blue parts indicate hydrophilic parts, with an intrinsic contact angle of 32.8 degrees.

100 to 240 in the channel, while the hydrophobic fluid filled the remaining space, and the same pressure was assigned at the inlet and outlet. The system was initially equilibrated during (typically) 10,000 time steps. We computed the velocity of fluids through a cross-section ($x = 60$), as shown in Figure S1 in the supplementary information. We can see that after 8000 time steps, the velocity evolved to achieve equilibrium. We therefore conclude that the system achieved an equilibrium state after 8000 time steps. We show a snapshot of fluid distributions in the channel in Figure 1 (a) at the 10,000th time step, after which the process of fluid flowback was simulated and evolution of the fluid flows in the channel was recorded as a function of time by decreasing the pressure at the outlet.

We studied the influence of particle surface wettability on the fluids flowing in the channel. Two well-defined types of wettability-patterned surface are shown in Figure 1 (b) and (c) and we performed simulations with mixtures of hydrophilic and hydrophobic particles. The mixed forms are shown in Figure 1 (d). For comparison, we also performed simulations with fully hydrophobic and fully hydrophilic particles. In the simulations, the intrinsic contact angle of the hydrophilic surface was about 32.8 degrees and the intrinsic contact angle of the hydrophobic surface was about 117.7 degrees. The channel wall was hydrophilic and had a contact angle of about 11.4 degrees. (Simulation details are shown in the supporting information.)

Results

When we reduced the pressure at the outlet, fluids flowback began. The evolution of the hydrophobic fluid flow through the cross-section ($x = 60$) for five cases was recorded and the velocity as a function of time is shown in Figure 2. It can be seen that the velocities first increase and then decrease to various extents. Fluctuations can clearly be seen in the patterned-wettability cases and the mixed case, where the hydrophobic fluid drives the aqueous phase away from the porous medium. The velocities each finally achieve steady state after 100,000 time steps. However, for hydrophilic particles, the hydrophobic fluid velocity reduces to a very small value, meaning that the hydrophobic fluid is blocked by the aqueous phase.

Because particles with wettability-patterned surfaces significantly reduce the interaction between the aqueous phase and the particle surface, the aqueous phase in the hydrophobic region can be readily cleaned up. Our simulations confirm that a patterned surface can markedly enhance the ability of a hydrophobic fluid to break through water blocking in micro-scale pores.

Discussion

We have calculated the aqueous phase volume fraction in the pore space of the particle-packing region (denoted by S_w), namely from $x = 130$ to 210 lattice units in the channel. Figure 3 shows S_w changing with evolution time.

In all five cases, S_w began to decline after we reduced pressure at the outlet, and tended to be stable after about 50,000 time steps. The stable volume fractions for the five cases clearly differ. S_w for the hydrophilic particles was remarkably higher than for the other four cases, meaning that there was more aqueous phase entrapped within the porous region. Because the hydrophilic regions of wettability-patterned particles retained a small quantity of aqueous phase adjacent to the channel wall, S_w was in the medium range. Conversely, the fully hydrophobic particle eliminated most of the aqueous phase and displayed the greatest conductivity. This explains why the fully hydrophobic particle shows the largest hydrophobic fluid velocity in Figure 2. Meanwhile, the volume fractions of the wettability-patterned particles in Figure 1(b) and 1(c) and the mixed case in Figure 1(d) are almost the same, so that the three cases had similar conductivity and display the same fluid velocity in Figure 2. Images illustrating the analyses above can be found in Figure 4.

To display the distribution of entrapped aqueous phase in the particle-packing medium, snapshots of a cross-section along the x axis at $y = 60$ at different times (0, 10,000, 50,000, 100,000, 150,000, 170,000) are shown for all five cases in Figure 4. All the systems were in the equilibrium state at $t = 0$. It is clear that some aqueous phase

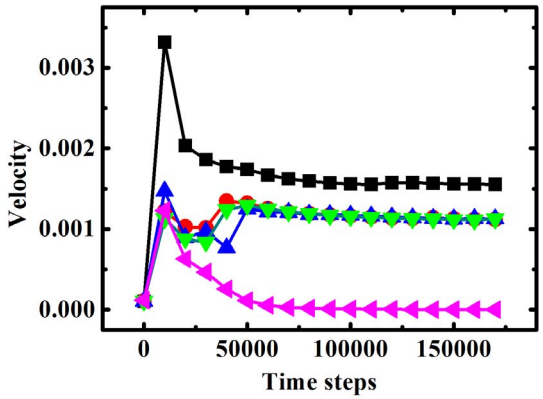

Figure 2 | **Comparison of the velocity of hydrophobic fluid through a cross-section ($x = 60$) for different cases.** Black solid squares (■), red solid circles (●), blue triangles (▲), green inverted triangles (▼) and magenta left triangles (◀) correspond to hydrophobic particles, particles modified as in Figure 1 (b), particles modified as in Figure 1 (c), mixed hydrophobic and hydrophilic particles, and hydrophilic particles, respectively.

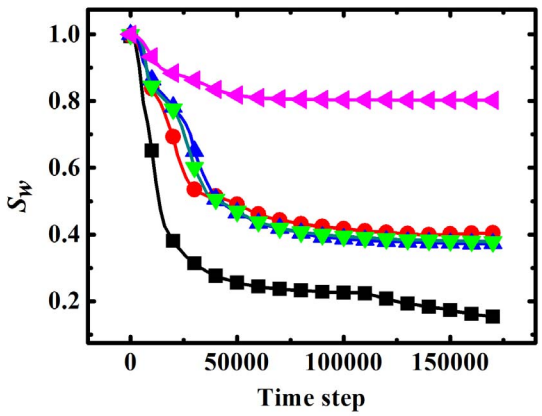

Figure 3 | Volume fraction in the particle-packing region changing with evolution time. Black solid squares (■), red solid circles (●), blue triangles (▲), green inverted triangles (▼) and magenta left triangles (◀) correspond to hydrophobic particles, particles modified as in Figure 1 (b), particles modified as in Figure 1 (c), mixed hydrophobic and hydrophilic particles, and hydrophilic particles, respectively.

near the particles formed water blocking in each case. With system evolution, the hydrophobic fluids flowed towards the particle-packing regions. At the 10,000th time step, we can see that the hydrophobic fluid had driven the aqueous phase inside the micro-scale pores in all cases. At the 50,000th time step, the hydrophobic fluid had broken through the particle-packing medium for particles with hydrophobic surfaces (a), patterned surfaces (b) and mixed hydrophobic and hydrophilic particles (d). At the 100,000th time step, for particles with hydrophobic surfaces (a), patterned surfaces (b) and (c), and mixed hydrophobic and hydrophilic particles (d), the hydrophobic fluids drove the aqueous phase out. For case (e), the hydrophobic fluid was blocked by the aqueous phase near the particles. At the 150,000th time step, in both cases (a) and (b), the hydrophobic fluids broke through the water blocking and flowed out of the channel. At the 170,000th time step, in both cases (c) and (d), the hydrophobic fluids also broke through the water blocking. However, in case (e), where hydrophilic particles were used, the hydrophobic fluid could not break through. In cases (b), (c) and (d), the hydrophobic regions were the same as the hydrophilic regions on the particle surfaces, whereas the times that hydrophobic fluid broke through water blocking differed. This indicates that the particles in Figure 1(b) were more effective with respect to hydrophobic fluid breakthrough. To understand the distribution of immiscible fluids in the pore space of case (b), we have drawn snapshots of the cross-section ($x = 150$) at different times in Figure 5.

Figure 5 gives the details of distribution of immiscible fluids in the micro-scale pores for case (b). We can see that the hydrophobic fluid started to open up micro-channels in the hydrophobic region of the center particles at the 4,200th time step. The micro-channels grew rapidly and covered almost all hydrophobic regions of the center particle along with the hydrophobic fluid penetration. At the 8,000th time step, new micro-channels began to form on the hydrophobic region of the outermost particles. Meanwhile, the middle micro-channels extended outwards and after uniting to form vertical micro-channels at the 8,200th time step, they gradually broadened, even extending into the hydrophilic regions, and spread into the spaces near the channel wall at the 10,000th time step. The micro-channels achieved steady state at about the 100,000th time step. In the hydrophobic region, the interaction between the aqueous phase and solid wall becomes weak and the hydrophobic fluid can easily remove the aqueous phase from hydrophobic regions, until the hydrophobic fluid breaks through the water blocking and flow out of the channel (shown in Figure 4).

In summary, using a 3D model including a channel and particles having surfaces with different wetting behaviors, we show that, in contrast to hydrophilic particles, wettability-patterned particles weaken the attractive forces between the aqueous phase and the particle surface and enhance channel conductivity for the hydrophobic fluid. For hydraulic fracturing used in the recovery of oil and gas, use of proppant particles with hydrophobic and hydrophilic patterned surfaces, is expected to eliminate water blocking. This work enriches our understanding of multiphase flows in porous media at the pore scale and fracture conductivity. It is very important to study oil/gas permeation in rock fractures, and is significant for the exploitation of low permeability reservoirs and shale gas.

Methods

The lattice Boltzmann method is well-suited to simulate the movement of fluids through porous networks[9–18]. We used the Shan–Chen multi-component multi-phase model[19,20] to study gas/oil flow through an idealized porous medium in micro-scale pores. This model involves a single relaxation time in the Bhatnagar–Gross–Krook (BGK) collision operator[21]. The time evolution of the σ th component in this model can be written as

$$f_i^\sigma(\boldsymbol{x}+\boldsymbol{c}_i\Delta t, t+\Delta t) - f_i^\sigma(\boldsymbol{x},t) = -\frac{1}{\tau^\sigma}\left[f_i^\sigma(\boldsymbol{x},t) - f_i^{\sigma,eq}(\boldsymbol{x},t)\right], \quad (1)$$

where Δt is the time step, $f_i^\sigma(\boldsymbol{x},t)$ is the density distribution function of the σ th component in direction $\mathbf{c}_i$ at $\boldsymbol{x}$, $f_i^{\sigma,eq}(\boldsymbol{x},t)$ is the equilibrium distribution function of the σ th component. τ^σ is the relaxation time of the σ th component characterizing the collision processes by which the distribution functions relax towards their equilibrium distributions.

In the three-dimensional nineteen-velocity model, the equilibrium distribution function, $f_i^{\sigma,eq}(\boldsymbol{x},t)$, depends only on local density and velocity and can be chosen as having following form:

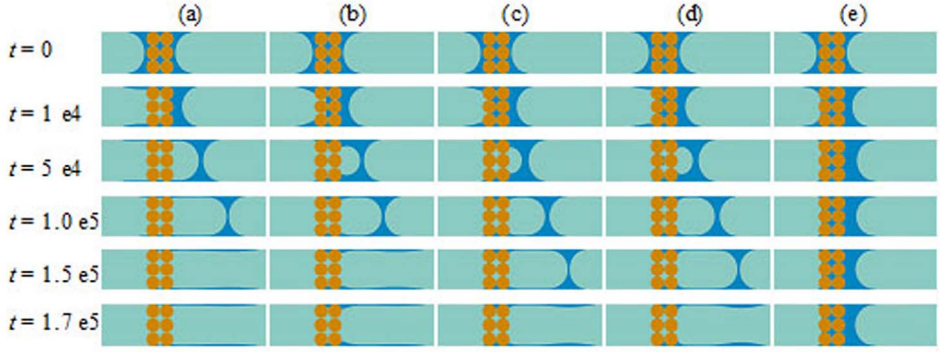

Figure 4 | Snapshots of the fluid distributions for differing particle wettability and evolution time. (a) The case with fully hydrophobic particles. (b) The case with wettability-patterned particles as in Figure 1b. (c) The case with wettability-patterned particles as in Figure 1c. (d) The case with hydrophobic and hydrophilic particles mixed as in Figure 1d. (e) The case with fully hydrophilic particles.

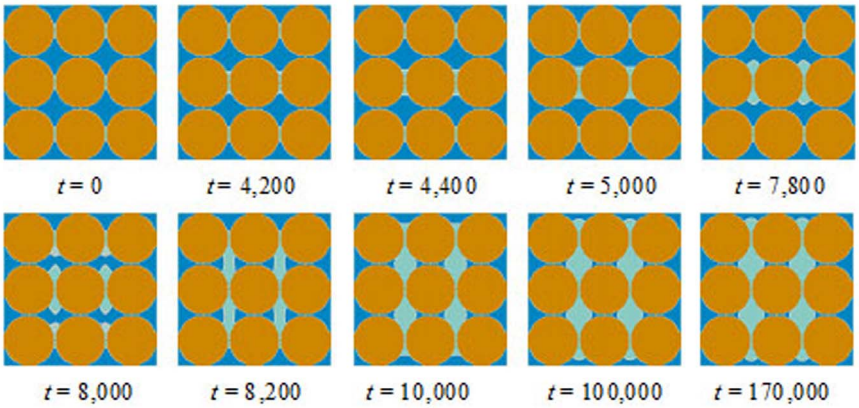

Figure 5 | Snapshots of a cross-section ($x = 150$) at different times for particles with two hydrophilic and two hydrophobic regions as in Figure 1b.

$$f_i^{\sigma,eq} = \omega_i \rho^\sigma \left[1 + \frac{(\mathbf{c}_i \cdot \mathbf{u}^{\sigma,eq})}{c_s^2} + \frac{(\mathbf{c}_i \cdot \mathbf{u}^{\sigma,eq})^2}{2c_s^4} - \frac{(\mathbf{u}^{\sigma,eq} \cdot \mathbf{u}^{\sigma,eq})}{2c_s^2}\right], \quad (2)$$

where the discrete velocities are

$$\boldsymbol{c}_i = \begin{cases} (0,0,0)c & i=0 \\ (\pm 1,0,0)c, (0,\pm 1,0)c, (0,0,\pm 1)c & i=1,\ldots,6 \\ (\pm 1,\pm 1,0)c, (\pm 1,0,\pm 1)c, (0,\pm 1,\pm 1)c & i=7,\ldots,18 \end{cases}, \quad (3)$$

and the weight factors are

$$\omega_i = \begin{cases} 1/3 & i=0 \\ 1/18 & i=1,2,\cdots,6 \\ 1/36 & i=7,8,\cdots,18 \end{cases}. \quad (4)$$

The mass density ρ^σ and momentum density $\rho^\sigma \mathbf{u}^\sigma$ of each component fluid are calculated for each node via the following equations

$$\rho^\sigma = \sum_i f_i^\sigma, \quad (5)$$

$$\rho^\sigma \mathbf{u}^\sigma = \sum_i \mathbf{c}_i f_i^\sigma. \quad (6)$$

The relaxation time tunes the kinematic viscosity of the σ th component by

$$\nu^\sigma = (\tau^\sigma - \frac{1}{2}) c_s^2 \Delta t. \quad (7)$$

The interactions between gas, liquid and rock control the flow and distribution of fluids in porous media[22–26]. In the Shan–Chen multiphase model, the fluid-fluid interaction, which is proportional to the product of a function of the particle number densities, can be written as

$$\boldsymbol{F}_l^\sigma(\boldsymbol{x}) = -G_c \rho^\sigma(\boldsymbol{x},t) \sum_i w_i \rho^{\overline{\sigma}}(\boldsymbol{x} + \boldsymbol{c}_i \Delta t, t) \boldsymbol{c}_i, \quad (8)$$

where $\boldsymbol{F}_l^\sigma(\boldsymbol{x})$ is the fluid-fluid interaction force, and the strength of two-phase interaction is denoted by G_c, which is negative and represents the attraction between the two phases. σ and $\overline{\sigma}$ denote two different fluid components, respectively. w_i is a weight factor, depending on the velocity model. It is simple to describe the interaction between a fluid and a wall by introducing an extra interaction force, and this method is first used by Martys and Chen[27]. The idea is to create an analogue to the particle-particle interaction force used to induce phase separation, and it is described as

$$\boldsymbol{F}_{ads}^\sigma(\boldsymbol{x}) = -G_{ads}^\sigma \rho^\sigma(\boldsymbol{x},t) \sum_i w_i s(\boldsymbol{x} + \boldsymbol{c}_i \Delta t, t) \boldsymbol{c}_i, \quad (9)$$

where s = 0 or 1 for the fluid and the solid phases, respectively. The interaction strength between each fluid and solid surface was adjusted by the parameter G_{ads}^σ. In the simulation, the hydrophilic and hydrophobic regions of the solid particles have different adhesion parameter G_{ads}^σ. The intrinsic contact angle of the hydrophobic regions is 117.7 degrees, whereas the intrinsic contact angle of the hydrophilic regions is 32.8 degrees.

The macroscopic velocity $\boldsymbol{u}^{\sigma,eq}$ of the σ th component in the multiphase model is defined by

$$\boldsymbol{u}^{\sigma,eq} = \boldsymbol{u}' + \frac{\tau^\sigma (\boldsymbol{F}_l^\sigma + \boldsymbol{F}_{ads}^\sigma)}{\rho^\sigma}, \quad (10)$$

where $\mathbf{u}'$ is the lattice velocity, defined as

$$\boldsymbol{u}' = \frac{\sum_\sigma \frac{1}{\tau^\sigma} \sum_i \boldsymbol{c}_i f_i^\sigma}{\sum_\sigma \frac{1}{\tau^\sigma} f_i^\sigma}. \quad (11)$$

The averaged fluid momentum before and after collision is[28]

$$\rho \boldsymbol{u} = \rho \boldsymbol{u}^\sigma + \frac{1}{2} \sum_\sigma \boldsymbol{F}^\sigma, \quad (12)$$

where $\boldsymbol{u}$ is the overall fluid velocity, and $\rho = \sum_\sigma \rho^\sigma$ is the total mass density of the whole fluid. The pressure of the whole fluid is given by[28]

$$P(\boldsymbol{x}) = c_s^2 \sum_\sigma \rho^\sigma(\boldsymbol{x}) + \frac{G_c}{3} \rho^\sigma(\boldsymbol{x}) \rho^{\overline{\sigma}}(\boldsymbol{x}). \quad (13)$$

The Shan–Chen model modifies the equilibrium velocity in the collision operator to include an interactive force, and thus it can realize phase separation and surface-tension effects[29]. The wettability of the solid surface (particle and channel) can be obtained by adjusting the liquid-solid interaction[30–32]. Different contact angles are obtained through adjusting the G_{ads}^σ, as shown in Supplementary Figure S2. The evolution computation is parallelized using a Message Passing Interface (MPI). The model has been successfully applied in many multiphase investigations, such as contact angle[30,33], contact line dynamics[34,35], and the effects of wall wettability, topography and micro-structure on drag reduction for fluid flow through micro-channels[36].

1. Mirzaei-Paiaman, A. & Masihi, M. Scaling equations for oil/gas recovery from fractured porous media by counter-current spontaneous imbibition: from development to application. *Energ. Fuel.* **27**, 4662–4676 (2013).
2. Holditch, S. Factors affecting water blocking and gas flow from hydraulically fractured gas wells. *J. Petrol. Technol.* **31**, 1515–1524 (1979).
3. Bennion, D. B., Bietz, R. F. & Thomas, F. B. Reductions in the productivity of oil and low permeability gas reservoirs due to aqueous phase trapping. *J. Can. Petrol. Technol.* **33**, 45–54 (1994).
4. Bennion, D. B., Thomas, F. B., Bietz, R. F. & Bennion, D. W. Water and hydrocarbon phase trapping in porous media-diagnosis, prevention and treatment. *J. Can. Petrol. Technol.* **35**, 29–36 (1996).
5. Bennion, D. B. & Thomas, F. B. Formation damage issues impacting the productivity of low permeability, low initial water saturation gas producing formations. *J. Energ. Res. Technol.* **127**, 240–247 (2005).
6. Wang, C. *et al.* Stable liquid water droplet on a water monolayer formed at room temperature on ionic model substrates. *Phys. Rev. Lett.* **103**, 137801 (2009).
7. Cheh, J., Gao, Y., Wang, C., Zhao, H. & Fang, H. Ice or water: thermal properties of monolayer water adsorbed on a substrate. *J. Stat. Mech. Theory E.* **2013**, P06009 (2013).
8. Luo, C. *et al.* Direct Three-Dimensional Imaging of the Buried Interfaces between Water and Superhydrophobic Surfaces. *Angew. Chem. Int. Ed.* **49**, 9145–9148 (2010).
9. Succi, S., Benzi, R. & Higuera, F. The lattice Boltzmann equation: a new tool for computational fluid-dynamics. *Physica D.* **47**, 219–230 (1991).
10. Guo, Z. & Zhao, T. Lattice Boltzmann model for incompressible flows through porous media. *Phys. Rev. E* **66**, 036304 (2002).
11. Rama, P. *et al.* Multiscale modeling of single-phase multicomponent transport in the cathode gas diffusion layer of a polymer electrolyte fuel cell. *Energ. Fuel.* **24**, 3130–3143 (2010).
12. Guo, Z. & Zhao, T. A lattice Boltzmann model for convection heat transfer in porous media. *Numer. Heat Transfer, Part B* **47**, 157–177 (2005).

13. Chen, S. & Doolen, G. D. Lattice Boltzmann method for fluid flows. *Annu. Rev. Fluid. Mech.* **30**, 329–364 (1998).
14. Martys, N. S. & Chen, H. Simulation of multicomponent fluids in complex three-dimensional geometries by the lattice Boltzmann method. *Phys. Rev. E* **53**, 743–750 (1996).
15. Huang, H., Wang, L. & Lu, X. Evaluation of three lattice Boltzmann models for multiphase flows in porous media. *Comput. Math. Appl.* **61**, 3606–3617 (2011).
16. Huang, H. & Lu, X. Relative permeabilities and coupling effects in steady-state gas-liquid flow in porous media: A lattice Boltzmann study. *Phys. Fluids* **21**, 092104–092110 (2009).
17. Gan, Y., Xu, A., Zhang, G., Li, Y. & Li, H. Phase separation in thermal systems: A lattice Boltzmann study and morphological characterization. *Phys. Rev. E* **84**, 046715 (2011).
18. Wang, L. & Afsharpoya, B. Modeling fluid flow in fuel cells using the lattice-Boltzmann approach. *Math. Comput. Simulat.* **72**, 242–248 (2006).
19. Shan, X. & Chen, H. Lattice Boltzmann model for simulating flows with multiple phases and components. *Phys. Rev. E* **47**, 1815–1819 (1993).
20. Shan, X. & Chen, H. Simulation of nonideal gases and liquid-gas phase transitions by the lattice Boltzmann equation. *Phys. Rev. E* **49**, 2941–2948 (1994).
21. Qian, Y., d' Humieres, D. & Lallemand, P. Lattice BGK Models for Navier-Stokes Equation. *Europhys. Lett.* **17**, 479–484 (1992).
22. Genty, A. & Pot, V. Numerical Simulation of 3D Liquid–Gas Distribution in Porous Media by a Two-Phase TRT Lattice Boltzmann Method. *Transport Porous. Med.* **96**, 271–294 (2013).
23. Saraji, S., Goual, L. & Piri, M. Adsorption of asphaltenes in porous media under flow conditions. *Energ. Fuel.* **24**, 6009–6017 (2010).
24. Xu, Y., Liu, Y. & Huang, G. Lattice Boltzmann simulation of momentum and energy transfer in a porous medium. *Mod. Phys. Lett. B* **19**, 1531–1534 (2005).
25. Yan, W., Liu, Y., Guo, Z. & Xu, Y. Lattice Boltzmann simulation on natural convection heat transfer in a two-dimensional cavity filled with heterogeneously porous medium. *Int. J. Mod. Phys. C* **17**, 771–783 (2006).
26. Gao, H., Han, J., Jin, Y. & Wang, L. Modelling microscale flow and colloid transport in saturated porous media. *Int. J. Comput. Fluid. D.* **22**, 493–505 (2008).
27. Martys, N. S. & Chen, H. Simulation of multicomponent fluids in complex three-dimensional geometries by the lattice Boltzmann method. *Phys. Rev. E* **53**, 743–750 (1996).
28. Kang, Q., Zhang, D. & Chen, S. Displacement of a two-dimensional immiscible droplet in a channel. *Phys. Fluids* **14**, 3203–3214 (2002).
29. Aidun, C. K. & Clausen, J. R. Lattice Boltzmann Method for Complex Flows. *Annu. Rev. Fluid. Mech.* **42**, 439–472 (2010).
30. Huang, H., Thorne, J. D. T., Schaap, M. G. & Sukop, M. C. Proposed approximation for contact angles in Shan-and-Chen-type multicomponent multiphase lattice Boltzmann models. *Phys. Rev. E* **76**, 1–6 (2007).
31. Zhang, R., Di, Q., Wang, X., Ding, W. & Gong, W. Numerical study of the relationship between apparent slip length and contact angle by Lattice Boltzmann Method. *J. Hydrodyn.* **24**, 535–540 (2012).
32. Dou, Z., Zhou, Z. & Sleep, B. Influence of wettability on interfacial area during immiscible liquid invasion into a 3D self-affine rough fracture: Lattice Boltzmann simulations. *Adv. Water Resour.* **61**, 1–11 (2013).
33. Guo, H. & Fang, H. Drop size dependence of the contact angle of nanodroplets. *Chin. Phys. Lett.* **22**, 787–790 (2005).
34. Fang, H., Fan, L., Wang, Z., Lin, Z. & Qian, Y. Studying the contact point and interface moving in a sinusoidal tube with lattice Boltzmann method. *Int. J. Mod. Phys. B* **15**, 1287–1303 (2001).
35. Fan, L., Fang, H. & Lin, Z. Simulation of contact line dynamics in a two-dimensional capillary tube by the lattice Boltzmann model. *Phys. Rev. E* **63**, 051603 (2001).
36. Zhang, R., Di, Q., Wang, X. & Gu, C. Numerical study of wall wettabilities and topography on drag reduction effect in micro-channel flow by Lattice Boltzmann Method. *J. Hydrodyn.* **22**, 366–372 (2010).

Acknowledgments

The authors thank Drs Rongzheng Wan, Jige Chen, Meng Zhang and Chunlei Wang for helpful discussions and comments. This work is partially supported by National Natural Science Foundation of China (Grant Nos. 11290164, 11362003 and U1262109).

Author contributions

H.P.F. contributed most of the ideas. H.P.F., R.L.Z., B.H.W. and N.S. designed simulations. R.L.Z. performed most of the numerical simulations. H.P.F., Y.S.X. and R.L.Z. carried out theoretical analysis. H.P.F., Y.S.X., B.H.W. and R.L.Z. wrote the paper. All authors discussed the results and commented on the manuscript.

Additional information

Supplementary information accompanies this paper at http://www.nature.com/scientificreports

Competing financial interests: The authors declare no competing financial interests.

How to cite this article: Zhang, R.L., Xu, Y.S., Wen, B.H., Sheng, N. & Fang, H.P. Enhanced Permeation of a Hydrophobic Fluid through Particles with Hydrophobic and Hydrophilic Patterned Surfaces. *Sci. Rep.* **4**, 5738; DOI:10.1038/srep05738 (2014).